



Universidad Autónoma
de Madrid

Biblos-e Archivo
Repositorio Institucional UAM

Repositorio Institucional de la Universidad Autónoma de Madrid

<https://repositorio.uam.es>

Esta es la **versión de autor** del artículo publicado en:
This is an **author produced version** of a paper published in:

Nanoscale 11 (2018): 2317-2325

DOI: <https://doi.org/10.1039/c8nr08928k>

Copyright: © 2018 Royal Society of Chemistry

El acceso a la versión del editor puede requerir la suscripción del recurso

Access to the published version may require subscription

Pseudo-Ordered Distribution of Ir Nanocrystals on h-BN

Antonio J. Martínez-Galera ^{*a} and José M. Gómez-Rodríguez ^{a,b,c}

Received 00th January 20xx,
Accepted 00th January 20xx

DOI: 10.1039/x0xx00000x

www.rsc.org/

A 2D material consisting in a pseudo-ordered distribution of Ir nanocrystals supported on the h-BN/Rh(111) surface is presented here. This particular spatial distribution of the Ir nanoparticles is achieved thanks to the existence of a large variety of adsorption positions within the pores of this nanomesh template with hexagonal symmetry. The resulting deviations of nanoparticles positions with respect to a perfect hexagonal lattice, which confer this material a special interest in the field of optics, can be tuned by the temperature and the amount of Ir. Upon annealing, this material undergoes slight structural changes in the temperature range 370–570 K and much more drastic ones, due to cluster coalescence, between 670 and 770 K. This relatively high onset of coalescence is encouraging for using this 2D material as a catalyst for reactions as the oxidation of carbon monoxide or of nitrogen monoxide, which are especially relevant in the field of environmental science. Finally, metal nanostructures, exhibiting regular geometries have been created from this material by using the STM tip. Because of the insulating character of h-BN, these nanostructures could be very promising to design conductive nanotracks.

Introduction

Nanoparticles consisting of only a few atoms of metal elements are being object of intensive study due to their potential in fields as electronics,^{1, 2} optoelectronics,³ magnetism,^{4, 5} plasmonics,⁶ environmental science,⁷ energy production⁸ and storage⁹ or catalysis¹⁰ among others. Along the last two decades, one of the biggest challenges in the field of nanoparticles is being the use of ordered networks of these zero dimensional elements to enhance their efficiency and/or achieve new functionalities.^{1, 11–14} For instance, they are expected to allow for a more coordinated association of the individual clusters in parallel, offering a faster operation as well as the possibility of performing more complex tasks. It would increase the expectative of these materials to be implemented in tomorrow devices with applications in magnetism,^{15, 16} data storage,^{15, 16} energy conversion¹³ and catalysis^{13,17,18}. Likewise, the uniform inter-nanoparticle spacing is ideal to use these cluster superlattices to try to obtain a coherent response when interacting with light, an issue of special relevance in optics and plasmonics.^{11, 19–21} It also applies to nearly periodic nanoparticle distributions, which, under certain circumstances, can be even more convenient than perfectly periodic ones.^{19, 22} As an example, it is interesting to mention that, light absorption on graphene decorated with nanoparticles decreases as their arrangement approaches towards a perfectly periodic structure, when the average distances

between aggregates are smaller than 40 nm.²² Moreover, because of their regular or nearly regular geometry, nanoparticle arrays constitute an ideal platform for the development of nanostructures with well-defined customized geometries by means of top down approaches.²³ It could be of great interest to print small nanocontacts and conductive tracks, although in this case an insulating support is required. For most of these purposes the size and the shape of nanoparticles are key aspects,^{1, 16, 20, 24} and, hence, a similar size and a well-defined structure of the aggregates is an essential prerequisite. For all of the above mentioned, the development and characterization of novel composites consisting of ordered arrays of monodisperse size nanoparticles, either supported on a substrate or embedded into a matrix, has been, during the last two decades, and still it is, a hot topic in nanotechnology and in general, in materials science.^{1, 13, 14, 15} An important limitation, however, of those systems that hinders their implementation in products and services for society, is the tendency of nanoparticles to agglomerate into larger aggregates, effect that is accentuated when increasing the temperature.^{25–28} As a result they generally exhibit a low thermal stability; problem that needs to be solved, given the importance of the size and shape of nanoparticles in their properties.^{1, 16, 24}

The ideal system would be an ordered or pseudo-ordered array of monodisperse size nanoparticles with well-defined structure exhibiting a good thermal stability supported on a substrate. In most of the cases it is, in addition, convenient to use inert substrates to reduce their effects on the properties of nanoparticles. Interesting examples of inert supports are graphene and h-BN monolayers, which can be obtained on a large variety of substrates^{29–39} and admit different kinds of functionalization.^{40–45} A good approximation to this ideal scenario are the ordered arrays of single nanocrystals composed of only a few atoms of metal elements grown on graphene supports.^{26, 46–48} Nevertheless, these nanomaterials have two main points of weakness: 1) they exhibit a limited thermal stability,²⁶ and

^a Departamento de Física de la Materia Condensada, Universidad Autónoma de Madrid, E-28049 Madrid, Spain. E-mail: antonio.galera@uam.es

^b Condensed Matter Physics Center (IFIMAC), Universidad Autónoma de Madrid, E-28049 Madrid, Spain

^c Instituto Nicolás Cabrera, Universidad Autónoma de Madrid, E-28049 Madrid, Spain

Electronic Supplementary Information (ESI) available: Further details of the composition and structure of the material as well as about its thermal stability. See DOI: 10.1039/x0xx00000x

2) the conducting character of graphene, although interesting in some applications in optics,²² limits the versatility of these arrays, since their possible applications in nanoelectronics are hindered. For this reason, there is a great interest in the development of materials composed of a low-dimensional insulating substrate, such as hexagonal boron nitride (h-BN), and an ordered network of nanoparticles.^{49–53} The first of this kind of systems was obtained by Brihuega et al., who succeeded in the growth of a Co nanoparticle superlattice on the h-BN/Rh(111) surface.⁴⁹ After this work, there have been a few studies reporting the growth of various metal nanoparticles on different h-BN/metal surfaces.^{50–54} In all these cases nanoparticles are found preferentially on the nanomesh pores, or equivalently, on the moiré valleys resulting on the h-BN/metal surface. In the present work it is presented a nanoparticle network grown on a h-BN/metal surface, in which it is possible to have a significant degree of control in the positioning of the aggregates within the pores/valleys of the moiré supercell. Additionally, this work demonstrates that it is possible to manipulate such nanoparticles networks on the h-BN/Rh(111) surface by means of the STM tip.

Herein, a composite material consisting in a nearly ordered distribution of monodisperse size Ir nanocrystals supported on the h-BN/Rh(111) template is presented. This unique material combines the versatility of an inert and insulating support as is the case of h-BN with a high structural perfection as well as a significantly better thermal stability as compared to others previously reported high structural quality superlattices of nanocrystals with well-defined structure and monodisperse size grown on inert substrates. In addition, to the best of our knowledge, to date, it is the only one of this kind of related materials offering the possibility of fine tuning the deviation of the clusters positioning with respect to a perfectly periodic hexagonal lattice by regulating the amount of Ir supplied and the annealing temperature. This important feature, according to what mentioned above, could have important implications in plasmonics and optics.^{19, 22}

Experimental

Experiments were performed in an ultrahigh vacuum (UHV) system equipped with a homebuilt variable temperature scanning tunneling microscope (VT-STM)^{55, 56} for sample characterization and several standard facilities for sample preparation including a sputter gun and a heater. This system also has a combined 4-grid Low Energy Electron Diffraction (LEED)/Auger Electron Spectroscopy (AES) optics. With this device, AES measurements are performed by using a retarding field analyser (RFA). Rh(111) surfaces were prepared by a cycling procedure of Ar⁺ bombardment at an energy of the incident ions of 1 kV and annealing at 1120 K at an oxygen partial pressure of 2×10^{-6} Torr. Afterwards, the Rh(111) single crystal was annealed also at 1120 K without supplying O₂. A single layer of h-BN was grown by thermal decomposition of borazine (B₃H₆N₃). Specifically, the freshly prepared Rh(111) substrate kept at 1070 K was exposed to 50 L borazine at a partial pressure of 2.5×10^{-8} Torr. Ir was sublimated from a home built evaporator. It consists of a filament made out of an Ir wire of 0.25 mm diameter. A precise calibration of the sublimation rate on the basis of the filament current was performed by means of STM imaging after Ir deposition on a Rh(111) surface. Thus, the

values of the Ir coverage provided along the manuscript are referred to the atomic density of the (111) planes of the Rh crystal structure, i.e. $1\text{ML} = 1.6 \times 10^{19} \text{ m}^{-2}$.

STM measurements were carried out in the constant current mode with the bias voltage applied to the sample. WSxM software was employed for data acquisition and processing.⁵⁷ Prior to extract the apparent height histograms from the STM images, the spurious influence of the piezo creep along the vertical direction and of other non-linear effects was minimized by means of an improved version of the flatten plus utility included in the WSxM software.⁵⁸ Both apparent height and distances between first neighbors histograms were constructed by using codes specifically designed for those purposes. In order to measure more accurately both parameters, the convolution effects due to the finite size of the STM tip were avoided by taking as the values of the nanoparticles apparent heights those measured in the topmost point of the atomic aggregates.⁵⁹ Apparent height histograms were constructed from STM images obtained by using the same tunneling parameters ($V_s = +2.2 \text{ V}$ and $I_T = 0.4 \text{ nA}$), and only were considered those topographs, in which the apparent height of the nanomesh pores, as measured on cluster vacancies either naturally occurring or artificially created, was around 0.05 nm. Likewise, the distances between first neighbors nanoparticles were measured from the in-plane positions corresponding to the topmost point of the aggregates, and, only those clusters occupying immediately adjacent nanomesh pores were considered to construct the histograms.

Results and discussion

Figure 1 reveals the structure of the material presented here, which, as above mentioned, consists of Ir nanoparticles formed on the h-BN/Rh(111) surface (see Figure S1–S3 for further details). As a reference, a STM image acquired on the pristine h-BN/Rh(111) surface is shown in Figure 1a. The STM topographs in Figure 1b–d show a pronounced dependence of the spatial distribution of the nanoparticles over the h-BN/Rh(111) surface on the amount of Ir deposited. Specifically, the STM image in Figure 1b reveals that at lower coverages there is preferential adsorption on the pores of the nanomesh, which are periodically distributed according to a hexagonal superlattice, although only a fraction of them are occupied by nanoparticles. Figure 1b (upper panel) also shows that the adsorption site of the nanoparticles inside the pores is not unique, but they can be found centered at a large variety of positions (see also Figure 1e). When the Ir coverage increases, all of the pores become occupied by nanoparticles (Figure 1c, upper panel). Finally, for a coverage of 1.8 ML, coalescence of the aggregates starts to occur, as indicated by the yellow elliptic contour in Figure 1d (upper panel), and, hence, the density of nanoparticles becomes again smaller than the density of pores (see Figure S4 for further details). Likewise, STM has also proven to be a powerful tool to reveal important aspects relative to the structural properties of the aggregates. In particular, when representing in histograms the values measured of nanoparticle apparent heights, there is an almost perfect matching between the positions of the peaks and the distances between consecutive (111) planes of bulk Ir, as observed in Figure 1b–d (Lower panels). Initially, depending on the Ir coverage, clusters giving rise to peaks corresponding to apparent heights

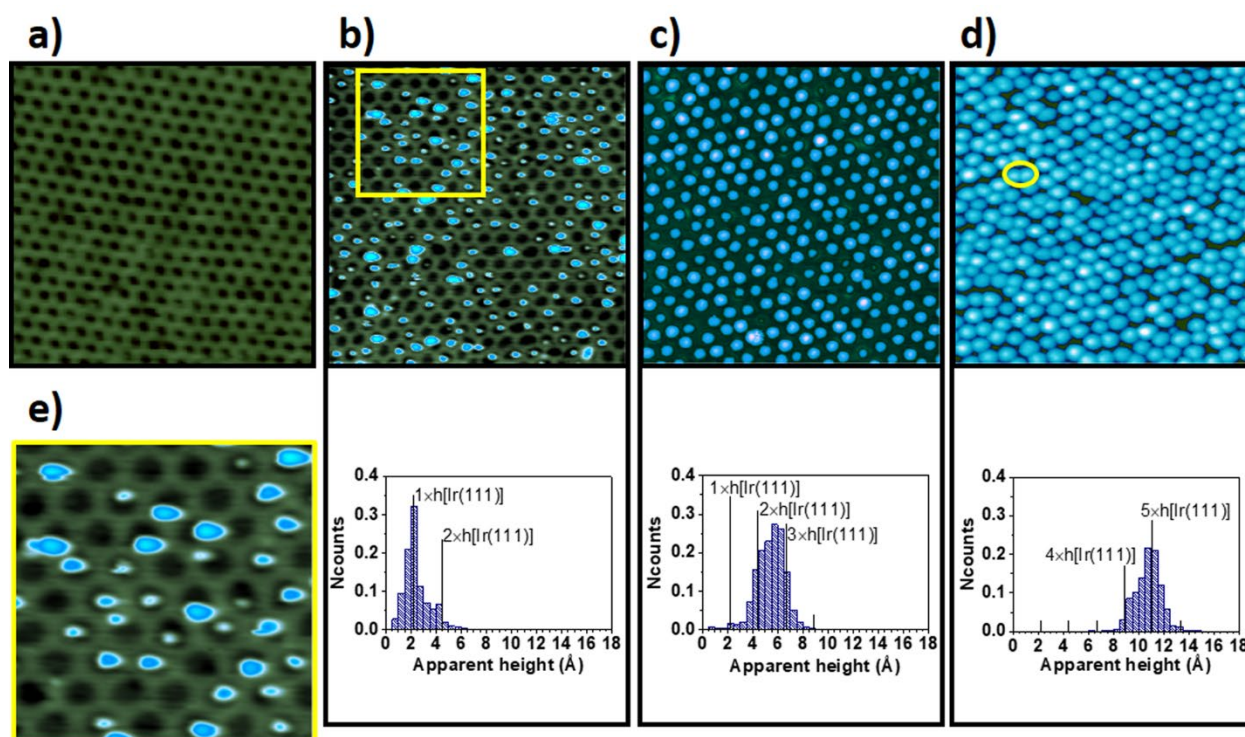


Figure 1. Evolution of clusters size, structure and distribution over the h-BN/Rh(111) surface with Ir coverage. **a)** Reference STM image acquired on the pristine h-BN/Rh(111) surface prior to the deposition of Ir. **b-d)** (Upper panels) STM topographs acquired after the deposition of **b)** 0.033 ± 0.007 , **c)** 0.30 ± 0.04 and **d)** 1.8 ± 0.2 ML Ir on h-BN/Rh(111). The yellow elliptic contour in Figure 1d indicates the position of an aggregate resulting from the coalescence of two nanoparticles. **e)** Digital zoom-in over the area of 20×20 nm² indicated by a yellow square in Figure 1b. Tunneling parameters: **a)** $V_s = +1.5$ V, $I_T = 0.34$ nA, **b)** $V_s = +2.2$ V, $I_T = 0.34$ nA, **c)** $V_s = +2.2$ V, $I_T = 0.4$ nA and **d)** $V_s = +2.2$ V, $I_T = 0.4$ nA. The size of the images displayed in **a)**-**d)** is 50×50 nm². **b-d)** (Lower panels) Apparent height histograms obtained from a number of STM images acquired, respectively, after the deposition of **b)** 0.033 ± 0.007 , **c)** 0.30 ± 0.04 and **d)** 1.8 ± 0.2 ML Ir on h-BN/Rh(111). N_{counts} represents the number of nanoparticles found with apparent heights within each bin normalized to the total number of aggregates analyzed in each histogram.

coincident with one, two and three times the interplanar spacing along the (111) direction of bulk Ir can be found (see histograms in Figure 1b,c). When coalescence starts to be appreciable, that is, at a coverage of around 1.8 ML, a peak centered on five times the distance between (111) planes of Ir dominates the histogram, although clusters giving rise to the peak of four times the interplanar distance are also present to a significant extent (see histogram in Figure 1d).

The interpretation of the results summarized in Figure 1 related to the spatial distribution of the nanoparticles together with those related to the interplanar distance and the cluster internal structure suggests the existence of three growth regimes. Regarding the first one, both the number of pores occupied by nanoparticles and the

sizes of these aggregates increase with the amount of Ir deposited on the h-BN/Rh(111) surface. Already for a coverage of 0.3 ML (see STM image in Figure 1c), all of the pores are occupied by nanoparticles. Then, a new regime, in which the density of clusters is constant while their sizes increase, is reached. The coverage range in which this growth regime is found is very broad. Therefore, by tuning the coverage it is possible to obtain different distributions with given apparent heights in the range between two and five times the distance between (111) planes of bulk Ir, in which roughly all of the pores are occupied by nanoparticles. For a coverage higher than 1.8 ML (see STM image in Figure 1d), cluster coalescence starts to happen. In this regime the size of the aggregates continues growing, but their density over the h-BN/Rh(111) surface decreases.

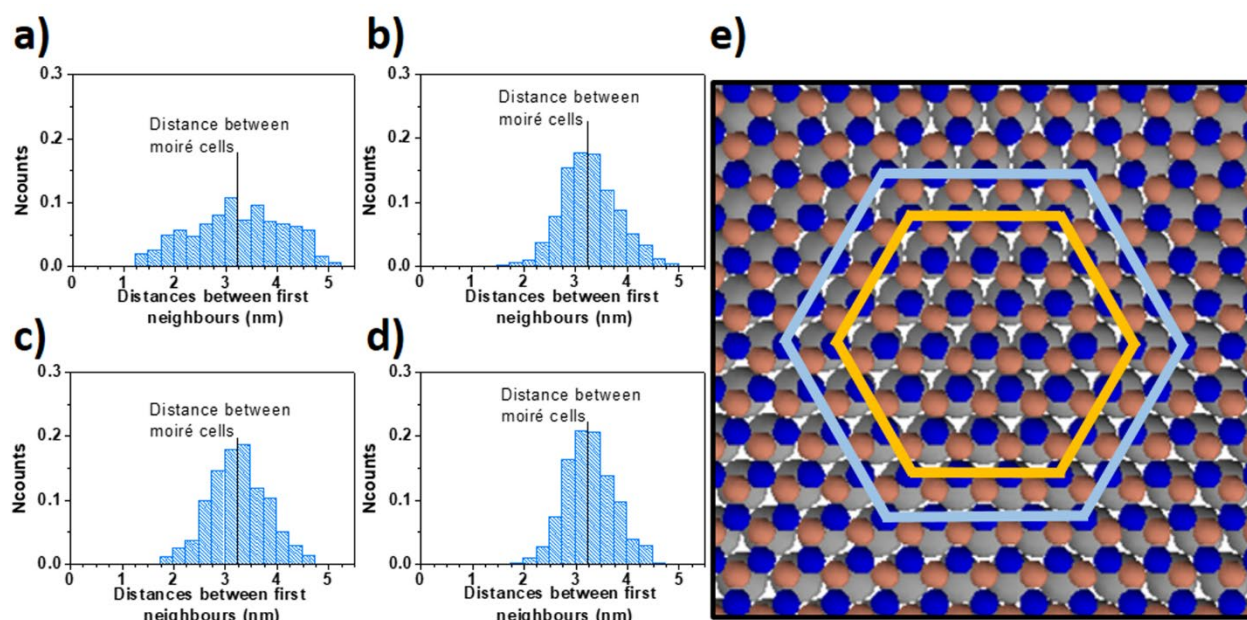


Figure 2. Quantification of the deviations of nanoparticles positions from a perfect hexagonal lattice. **a-d)** Histograms of distances between first neighbors clusters as measured on STM topographs acquired, respectively, for Ir coverages of a) 0.033 ± 0.007 , b) 0.30 ± 0.04 , c) 0.7 ± 0.1 and d) 1.8 ± 0.2 ML. N_{counts} represents the number of neighbor pairs separated by distances, whose values lie within each bin, normalized to the total number of aggregates analyzed in each histogram. **e)** Schematic representation indicating the limits of the restricted areas for positioning of the center of nanoparticles as extracted from the histograms for coverages of 0.033 ± 0.007 and 1.8 ± 0.2 ML Ir, which are represented, respectively, by a blue and a yellow hexagon.

From the side of the structure of clusters, special attention should be paid to the fact that, as observed in Figure 1b-d (Lower panels) as well as in Figure S3, the positions of the peaks in the apparent height histograms match to a reasonable extent with integer multiples of the interplanar distance along the (111) direction of bulk Ir. It points towards the fact that nanoparticles might exhibit a well-defined crystal structure consisting in stacks of atomic layers with an arrangement similar to that of the (111) planes of bulk Ir. Accordingly, on the basis of this argument, from the apparent height histograms shown in Figure 1 and S3 one could conclude that nanoparticles keep their crystalline structure regardless of the amount of Ir deposited until, at least, the early stages of the coalescence regime. Under such circumstances the maximum apparent height measured in the nanoparticles corresponds to five times the distance between consecutive (111) atomic planes. Note that the position of the histogram peak obtained for 0.3 ML (Figure 1c, lower panel) does not correspond to an integer multiple of the interplanar distance along the (111) direction of bulk Ir. In this case there are comparable amounts of nanoparticles with two and three Ir layers, and it seems that the peaks associated to both heights overlap due to their finite width, giving rise to a single broad peak centered around the middle between both.

As observed in the STM images shown in Figure 1b-e, clusters are not arranged according to a perfect hexagonal lattice defined by the periodicity of the nanomesh, but their positions exhibit small deviations associated to the different possibilities for nanoparticle adsorption within the pores. To quantify these deviations, histograms displaying the values of the distance between first neighbor nanoparticles have been constructed (see Figure 2a-d). The bin width has been chosen to match the lattice parameter of the h-BN lattice. In this way, each bin, as counted from the position indicated by the vertical black line, can be associated to an increment by one h-BN unit cell of the deviation of the distances between neighbors with respect to the case of a perfect hexagonal lattice with the periodicity of the nanomesh. As observed in Figure 2a-d, the histograms obtained at lower coverages become narrower by increasing the amount of Ir (see Figure S5 for further details). Specifically, at very low coverages the maximum/minimum distances found between two neighbor nanoparticles are the periodicity of the h-BN nanomesh plus/minus eight times the periodicity of the h-BN layer. On average, it corresponds to a maximum deviation, both to larger and to smaller values of the distance between first neighbors, of four unit cells of h-BN per nanoparticle. The maximum deviation decreases with increasing the amount of Ir until a coverage of around

Nanoscale

ARTICLE

0.6 ML Ir, where, on average, it takes a value of only three times the h-BN unit cell per aggregate. In other words, at lower coverages the positions of the centers of all of the nanoparticles must lie within a hexagon, centered on the pore, with a side length of four h-BN unit cells (indicated in light blue in Figure 2e). That area for nanoparticle positioning decreases with coverage until around 0.6 ML, where the side of the hexagon reaches a value of three times the lattice parameter of h-BN (indicated in yellow in Figure 2e). As observed in the histograms shown in Figure S5, that area is not further decreased by increasing the coverage even to around 3 ML Ir.

The first neighbor distances histograms demonstrate that the possible positions for the center of nanoparticles are restricted to a certain area centered on the nanomesh pores, whose lateral extent decreases with increasing coverage until 0.6 ML. This decrease is due to the fact that, apparently, there is a preference of nanoparticles giving rise to the maximum deviation, which are the ones located at the outer positions of the pore, to grow at larger sizes from their edges that are occupying the inner positions. Therefore, the central position of these nanoparticles shifts also towards inner positions within the pore. For most of the nanoparticles based systems analyzed by DFT calculations on the h-BN/Rh(111) nanomesh, the adsorption of the aggregates is energetically favored on the pores with respect to the wires.^{52-54,60} This preferential adsorption on the pores or, equivalently, on the valleys of the moiré superstructure has also been observed experimentally by means of STM imaging on several nanoparticles based systems growth on h-BN/metal surfaces.^{49, 51-54, 61} It could explain why the attachment of new Ir adatoms to nanoparticles located at outer positions of the pores of the h-BN/Rh(111) nanomesh takes place, preferentially, to the edges placed at inner locations within the pores rather than to those edges oriented towards the wires. The existence, in the present case, of a restricted area for nanoparticle positioning suggests that the aggregates do not extend over the whole pore at any Ir coverage even until, at least, the initial stages of coalescence. To conclude with the issue of the deviation of nanoparticle positioning with respect to a perfect hexagonal lattice, it is interesting to note that, as above mentioned, sometimes, pseudo-periodic structures can be even more convenient than perfectly periodic ones in terms of their response when interacting with light.^{19, 22}

An intrinsic limitation of substrate supported nanoparticles resides in the thermal stability, which is limited by coalescence.^{25, 26, 28} Figure 3 summarizes the results obtained in the study of the evolution of the size, shape and spatial distribution of clusters along sequential annealing at increasing temperatures (see also Figure S6, and S7 for further details). Specifically, Figure 3a-d shows representative STM topographs acquired on a sample resulting from the deposition of 0.7 ± 0.1 ML Ir on the h-BN/Rh(111) surface for a) prior to the beginning of an annealing sequence at increasing temperatures between 370 K and 970 K in intervals of 100 K and, after the annealing processes at

b) 570 K, c) 670 K and d) 970 K. The comparison of the STM images shown in Figure 3a and b reveals the absence of significant changes in the spatial distribution of the nanoparticles in the temperature range RT-570 K. However, as observed in Figure 3c, after the step at 670 K, some small vacancy islands with typical sizes between one and six units are formed. In turn, in the vicinity of such islands, the height of some of the nanoparticles increases (see yellow circles). Finally, Figure 3d shows that after the annealing step at 970 K only a small portion of the clusters as those observed prior to the beginning of the annealing sequence, which occupied just a single moiré cell, still survives.

Additional information was extracted from the analysis of the evolution of apparent height histograms extracted from STM images acquired along the sequential annealing processes. The histograms constructed from the same annealing sequence, in which the STM topographs displayed in Figure 3a-d were acquired, are shown in Figure 3e-h. The apparent height histograms become narrower with increasing the annealing temperature until the step at 570 K (see Figure 3e,f and S6a-d). Afterwards, as it can be appreciated in Figure 3g,h and S6e-h, the histograms undergo a gradual broadening as a consequence of cluster coalescence. Concretely, this coalescence is translated into the presence of peaks related to nanoparticles with higher apparent heights, which, already start to be visible after the step at 670 K. In this case the peak of five layers can be associated to the nanoparticles with increased size located in the vicinity of the vacancy islands (see Figure 3c).

The influence of annealing on the adsorption positions of the nanoparticles within the pores can be analyzed by means of histograms of distances between first neighbors. As observed in Figure 3i-k, the histograms become slightly narrower upon annealing until the step at 670 K. Here, it is noteworthy to mention that for the annealing sequence analyzed in Figure 3, the number of neighbor nanoparticles, which after their growth at RT gave rise to the values of the deviation of the distance between aggregates of five or more h-BN unit cells, becomes almost negligible after the annealing step at 570 K.

From the analysis of both apparent height and first neighbor distances histograms it can be concluded that this 2D material undergoes only slight structural changes upon annealing at temperatures in the range 370-570 K (see Figure 3 e,f and i,j in the main manuscript as well as Figure S6 a-d and S7 a-c in the supplementary information). In particular, the size distribution of the nanoparticles and that of their positions within the nanomesh pores are narrowed. In other words, these histograms reveal, on the one hand, an atomic redistribution taking place on the nanoparticles, resulting in an improvement of their size monodispersity (see Figure 3e,f and S6a-d), and, on the other hand, a decrease of the deviation of their positioning with respect to a perfectly periodic hexagonal superstructure (Figure 3 i,j and S7a-c). Further annealing induces

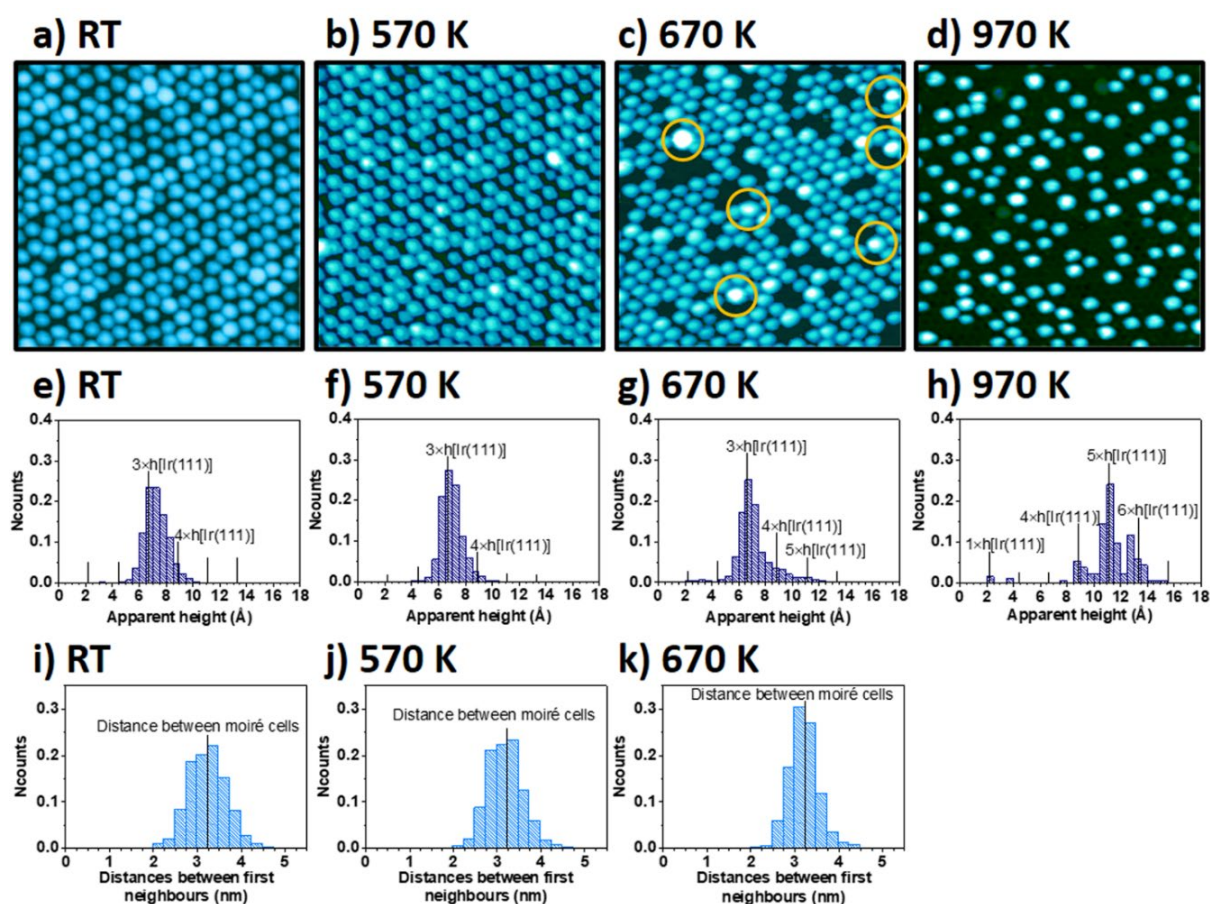


Figure 3. Evolution of clusters structure and distribution along annealing. **a-d)** STM topographs acquired on a sample resulting from the deposition of 0.7 ± 0.1 ML Ir on h-BN/Rh(111) **a)** prior to an annealing sequence at increasing temperatures in steps of 300 s in intervals of 100 K between 370 and 970 K and **b), c)** and **d)** after the annealing steps at 570 K, 670 K and 970 K, respectively. Tunneling parameters: $V_s = +2.2$ V, $I_T = 0.4$ nA; size 50×50 nm² for all of the topographs. **e-h)** Apparent height histograms extracted from a number of STM images acquired, respectively, prior to annealing the as grown sample and after the annealing steps at 570 K, 670 K and 970 K. Ncounts represents the number of nanoparticles found with apparent heights within each bin normalized to the total number of aggregates analyzed in each histogram. **i-k)** Histograms of distances between first neighbors nanoparticles as measured in STM images acquired **i)** prior to annealing and **j-k)** after the annealing steps at 570 K and 670 K, respectively. Ncounts represents the number of neighbor pairs separated by distances, whose values lie within each bin, normalized to the total number of aggregates analyzed in each histogram.

more drastic changes that occur from 670 K due to cluster coalescence as evidenced by the decrease in the structural perfection of the cluster network observed in STM images as well as in the broadening of the apparent height histograms.

For the 2D material presented here, the analysis of STM images, apparent height histograms and first neighbor distances histograms has demonstrated the absence of noticeable coalescence after annealing at temperatures as high as 570 K. After the annealing step at 670 K, cluster density starts to decrease at the same time that the average size of nanoparticles increases due to coalescence.

Therefore, the onset of coalescence must be between 570 and 670 K. It is encouraging to explore the possibility of using the Ir nanocrystals grown on the h-BN/Rh(111) system as catalyzers of important reactions from the point of view of the environmental science research as the oxidation by molecular oxygen of CO,⁶² which is also crucial in energy production by hydrogen fuel cells,⁶³ or of NO^{64, 65}. Therefore, the results obtained in this study are believed to stimulate further research in the field of catalysis. Here, it is also interesting to mention that the exposure of Pt nanocrystals on graphene/Ir(111) to radicals has proven to increase the thermal

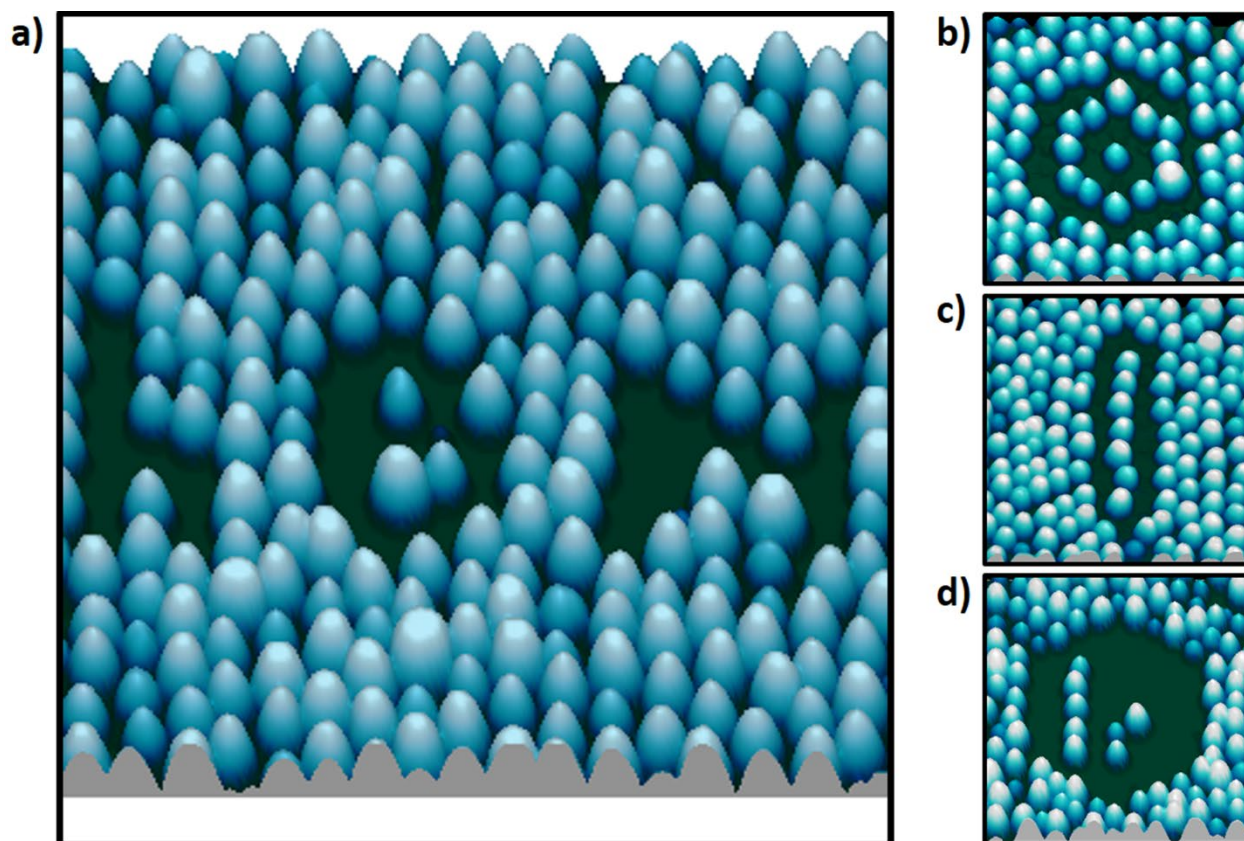


Figure 4. Nanomanipulation of clusters on the h-BN/Rh(111) surface. **a-d)** STM topographs acquired after the construction of nanostructures with regular geometries by removing Ir clusters by using the STM tip. Tunneling parameters: a) $V_s = +2.4$ V, $I_T = 0.3$ nA; size 48×43 nm², b) $V_s = +2.2$ V, $I_T = 0.2$ nA; size 30×30 nm², c) $V_s = +2.2$ V, $I_T = 0.2$ nA; size 35×35 nm² and d) $V_s = +2.2$ V, $I_T = 0.3$ nA; size 36×36 nm².

stability.⁵⁹ Similarly, the exposure to radicals could also further increase the thermal stability of the nanoparticles grown on h-BN/Rh(111), although this issue demands further research.

The development of metal nanostructures with tailored geometries over insulating substrates is an issue of special relevance in materials science. The material presented here consisting in a pseudo-ordered distribution of Ir nanocrystals grown on the insulating h-BN template offers an excellent platform to develop such nanostructures. The effective electrical isolation of nanoparticles from the metal Rh(111) substrate provided by the h-BN layer was previously demonstrated by Brihuega *et al.*, who observed that Co clusters grown on the h-BN/Rh(111) surface show the Coulomb gap expected for small metal clusters isolated from metallic electrodes.⁴⁹ For the Ir nanocrystals on h-BN/Rh(111), the average number of nanoparticles per nanomesh pore is roughly one in a broad range of Ir coverages. It ensures a regular intercluster spacing around the whole sample except for the small deviations (of the order of the nanoparticle size) of clusters positions with respect to a perfect hexagonal lattice,

which are insignificant as to affect the development of nanostructures with well-defined geometries. STM, due to its precision at the nanometer scale, is a perfect tool to construct nanostructures on surfaces. Thus, by using the STM tip to selectively remove Ir nanoparticles from the h-BN/Rh(111) template, the nanostructures shown in Figure 4 have been performed. Specifically, to remove each nanoparticle, after the acquisition of the STM image over a certain region, the piezo scan was stopped and the tip was placed over the aggregate to be removed. Afterwards, the tip was approached until contact towards the nanoparticle a vertical distance of typically 0.4–0.6 nm and, then, retracted back. This procedure gives rise to a nanoparticle vacancy on the chosen position. Therefore, this material could provide an ideal scenario for the development of electrical contacts with a perfect crystal structure and, hence with a well-defined geometry, as well as conductive tracks tailored at will to construct nanocircuits for electronic transport.

Conclusions

In summary, a two-dimensional material with pseudo-ordered structure made out of Ir nanocrystals has been grown by using as a template the hexagonal nanomesh resulting in the h-BN/Rh(111) interface. The pseudo-ordered structure of this material has been achieved thanks to the existence of a large variety of adsorption positions for the nanoparticles within the pores of the nanomesh. By increasing the amount of Ir, within the coverage range studied, on the h-BN/Rh(111) template, the maximum deviation of the positions of nanoparticles from the ones corresponding to a perfect hexagonal lattice decreases. This material exhibits only slight gradual structural changes in the temperature range 370–570 K consisting in a slight narrowing of the apparent height distribution of the aggregates as well as in a decrease in the deviation of the nanoparticle positioning with respect to a perfect hexagonal lattice. Annealing at higher temperatures, in the range of 570–670 K, results in more drastic structural changes due to cluster coalescence, consisting in a reduction of the order of the nanoparticle distribution and in a broadening of the apparent height distribution of the atomic aggregates. The tunability of the deviation of cluster positioning with respect to a perfect periodic structure with Ir coverage and/or with annealing temperature could offer the possibility to modify at will the interaction of this material with light. In addition, the onset of coalescence is high enough to encourage the use of these nanocrystals as catalysts for reactions as the oxidation of NO and of CO by molecular oxygen, which are of special interest in the fields of environmental science and, in the latter case also for energy production. Finally, nanostructures made out of Ir nanocrystals have been tailored with well-defined shapes by using the STM tip. Due to the fact that the h-BN support is an insulating material, small nanocontacts with well-defined crystal structure as well as conductive tracks electronically uncoupled from the local environment could be developed from this material.

Conflicts of interest

There are no conflicts to declare.

Acknowledgements

The authors acknowledge financial support from AEI and FEDER under project MAT2016-77852-C2-2-R (AEI/FEDER, UE). A.J.M.-G. acknowledges funding from the Spanish MINECO through the Juan de la Cierva program (ref. IJCI-2014-19209). The authors acknowledge Juan Manuel Pérez-Mato, Enrique Maciá and Tobias Stauber for fruitful discussions as well as Ignacio Horcas for the implementation of a new functionality in the WSxM software.

References

1. A. N. Shipway, E. Katz and I. Willner, *ChemPhysChem*, 2000, **1**, 18–52.
2. A. Kamyshny and S. Magdassi, *Small*, 2014, **10**, 3515–3535.
3. S. Coe, W. K. Woo, M. Bawendi and V. Bulovic, *Nature*, 2002, **420**, 800–803.
4. J. Bansmann, S. H. Baker, C. Binns, J. A. Blackman, J. P. Bucher, J. Dorantes-Davila, V. Dupuis, L. Favre, D. Kechrakos, A. Kleibert, K. H. Meiwes-Broer, G. M. Pastor, A. Perez, O. Toulemonde, K. N. Trohidou, J. Tuillon and Y. Xie, *Surf. Sci. Rep.*, 2005, **56**, 189–275.
5. G. C. Papaefthymiou, *Nano Today*, 2009, **4**, 438–447.
6. M. Pelton, J. Aizpurua and G. Bryant, *Laser Photon. Rev.*, 2008, **2**, 136–159.
7. A. K. Sinha, K. Suzuki, M. Takahara, H. Azuma, T. Nonaka and K. Fukumoto, *Angew. Chem.-Int. Edit.*, 2007, **46**, 2891–2894.
8. B. Oregan and M. Gratzel, *Nature*, 1991, **353**, 737–740.
9. P. Poizot, S. Laruelle, S. Grugeon, L. Dupont and J. M. Tarascon, *Nature*, 2000, **407**, 496–499.
10. D. Astruc, F. Lu and J. R. Aranzaes, *Angew. Chem.-Int. Edit.*, 2005, **44**, 7852–7872.
11. E. Hutter and J. H. Fendler, *Adv. Mater.*, 2004, **16**, 1685–1706.
12. S. Q. Liu and Z. Y. Tang, *J. Mater. Chem.*, 2010, **20**, 24–35.
13. J. Li, Y. C. Wang, T. Zhou, H. Zhang, X. H. Sun, J. Tang, L. J. Zhang, A. M. Al-Enizi, Z. Q. Yang and G. F. Zheng, *J. Am. Chem. Soc.*, 2015, **137**, 14305–14312.
14. K. J. Si, Y. Chen, Q. Q. Shi and W. L. Cheng, *Adv. Sci.*, 2018, **5**, 22.
15. J. Y. Cheng, C. A. Ross, V. Z. H. Chan, E. L. Thomas, R. G. H. Lammertink and G. J. Vancso, *Adv. Mater.*, 2001, **13**, 1174.
16. J. Y. Cheng, C. A. Ross, E. L. Thomas, H. I. Smith, R. G. H. Lammertink and G. J. Vancso, *IEEE Trans. Magn.*, 2002, **38**, 2541–2543.
17. A. Doron, E. Katz and I. Willner, *Langmuir*, 1995, **11**, 1313–1317.
18. C. R. Henry, *Catal. Lett.*, 2015, **145**, 731–749.
19. C. L. Haynes, A. D. McFarland, L. L. Zhao, R. P. Van Duyne, G. C. Schatz, L. Gunnarsson, J. Prikulis, B. Kasemo and M. Kall, *J. Phys. Chem. B*, 2003, **107**, 7337–7342.
20. K. C. Kao, H. Nishi and T. Tatsuma, *Phys. Chem. Chem. Phys.*, 2018, **20**, 3735–3740.
21. K. N'Konou, L. Peres and P. Torchio, *Plasmonics*, 2018, **13**, 297–303.
22. T. Stauber, G. Gomez-Santos and F. J. G. de Abajo, *Phys. Rev. Lett.*, 2014, **112**, 077401.
23. A. J. Martinez-Galera, I. Brihuega, A. Gutierrez-Rubio, T. Stauber and J. M. Gomez-Rodriguez, *Sci Rep.* 2014, **4**, 7314.
24. R. Narayanan and M. A. El-Sayed, *J. Phys. Chem. B*, 2005, **109**, 12663–12676.
25. F. Maillard, S. Schreier, M. Hanzlik, E. R. Savinova, S. Weinkauff and U. Stimming, *Phys. Chem. Chem. Phys.*, 2005, **7**, 385–393.
26. A. T. N'Diaye, T. Gerber, C. Busse, J. Myslivecek, J. Coraux and T. Michely, *New J. Phys.*, 2009, **11**, 103045.
27. A. Cao, R. Lu and G. Veser, *Phys. Chem. Chem. Phys.*, 2010, **12**, 13499–13510.
28. A. Cavallin, M. Pozzo, C. Africh, A. Baraldi, E. Vesselli, C. Dri, G. Comelli, R. Larciprete, P. Lacovig, S. Lizzit and D. Alfe, *ACS Nano*, 2012, **6**, 3034–3043.
29. C. Oshima and A. Nagashima, *J. Phys.-Condens. Matter*, 1997, **9**, 1–20.
30. M. Corso, W. Auwarter, M. Muntwiler, A. Tamai, T. Greber and J. Osterwalder, *Science*, 2004, **303**, 217–220.
31. A. B. Preobrajenski, A. S. Vinogradov and N. Martensson, *Surf. Sci.*, 2005, **582**, 21–30.
32. A. B. Preobrajenski, M. A. Nesterov, M. L. Ng, A. S. Vinogradov and N. Martensson, *Chem. Phys. Lett.*, 2007, **446**, 119–123.
33. E. Cavar, R. Westerstrom, A. Mikkelsen, E. Lundgren, A. S. Vinogradov, M. L. Ng, A. B. Preobrajenski, A. A. Zakharov and N. Martensson, *Surf. Sci.*, 2008, **602**, 1722–1726.

34. S. E. Harrison, M. A. Capano and R. Reifengerger, *Appl. Phys. Lett.*, 2010, **96**, 081905.
35. M. Batzill, *Surf. Sci. Rep.*, 2012, **67**, 83-115.
36. A. Martin-Recio, C. Romero-Muniz, A. J. Martinez-Galera, P. Pou, R. Perez and J. M. Gomez-Rodriguez, *Nanoscale*, 2015, **7**, 11300-11309.
37. M. Garnica, M. Schwarz, J. Ducke, Y. He, F. Bischoff, J. V. Barth, W. Auwärter and D. Stradi, *Phys. Rev. B*, 2016, **94**, 155431.
38. H. Gonzalez-Herrero, P. Pou, J. Lobo-Checa, D. Fernandez-Torre, F. Craes, A. J. Martinez-Galera, M. M. Ugeda, M. Corso, J. Enrique Ortega, J. M. Gomez-Rodriguez, R. Perez and I. Brihuega, *ACS Nano*, 2016, **10**, 5131-5144.
39. M. Schwarz, A. Riss, M. Garnica, J. Ducke, P. S. Deimel, D. A. Duncan, P. K. Thakur, T.-L. Lee, A. P. Seitsonen, J. V. Barth, F. Allegretti and W. Auwärter, *ACS Nano*, 2017, **11**, 9151-9161.
40. M. Telychko, P. Mutombo, M. Ondracek, P. Hapala, F. C. Bocquet, J. Kolorenc, M. Vondracek, P. Jelinek and M. Svec, *ACS Nano*, 2014, **8**, 7318-7324.
41. M. L. Ng, A. Shavorskiy, C. Rameshan, A. Mikkelsen, E. Lundgren, A. Preobrajenski and H. Bluhm, *ChemPhysChem*, 2015, **16**, 923-927.
42. M. Telychko, P. Mutombo, P. Merino, P. Hapala, M. Ondracek, F. C. Bocquet, J. Sforzini, O. Stetsovych, M. Vondracek, P. Jelinek and M. Svec, *ACS Nano*, 2015, **9**, 9180-9187.
43. A. J. Martinez-Galera, U. A. Schröder, F. Huttman, W. Jolie, F. Craes, C. Busse, V. Caciuc, N. Atodiresei, S. Bluegel and T. Michely, *Nanoscale*, 2016, **8**, 1932-1943.
44. U. A. Schröder, E. Granas, T. Gerber, M. A. Arman, A. J. Martinez-Galera, K. Schulte, J. N. Andersen, J. Knudsen and T. Michely, *Carbon*, 2016, **96**, 320-331.
45. U. A. Schröder, M. Petrovic, T. Gerber, A. J. Martinez-Galera, E. Granas, M. A. Arman, C. Herbig, J. Schnadt, M. Kralj, J. Knudsen and T. Michely, *2D Mater.*, 2017, **4**, 015013.
46. A. T. N'Diaye, S. Bleikamp, P. J. Feibelman, T. Michely, *Phys. Rev. Lett.*, 2006, **97**, 215501.
47. D. Franz, S. Runte, C. Busse, S. Schumacher, T. Gerber, T. Michely, M. Mantilla, V. Kilic, J. Zegenhagen, A. Stierle, *Phys. Rev. Lett.*, 2013, **110**, 065503.
48. D. Franz, N. Blanc, J. Coraux, G. Renaud, S. Runte, T. Gerber, C. Busse, T. Michely, P. J. Feibelman, U. Hejral, A. Stierle, *Phys. Rev. B*, 2016, **93**, 045426.
49. I. Brihuega, C. H. Michaelis, J. Zhang, S. Bose, V. Sessi, J. Honolka, M. A. Schneider, A. Enders and K. Kern, *Surf. Sci.*, 2008, **602**, L95-L99.
50. M. L. Ng, A. B. Preobrajenski, A. S. Vinogradov and N. Martensson, *Surf. Sci.*, 2008, **602**, 1250-1255.
51. J. Zhang, V. Sessi, C. H. Michaelis, I. Brihuega, J. Honolka, K. Kern, R. Skomski, X. Chen, G. Rojas and A. Enders, *Phys. Rev. B*, 2008, **78**, 165430.
52. M. C. Patterson, B. F. Habenicht, R. L. Kurtz, L. Liu, Y. Xu and P. T. Sprunger, *Phys. Rev. B*, 2014, **89**, 205423.
53. M. Will, N. Atodiresei, V. Caciuc, P. Valerius, C. Herbig and T. Michely, *ACS Nano*, 2018, **12**, 6871-6880.
54. W. C. McKee, M. C. Patterson, J. R. Frick, P. T. Sprunger and Y. Xu, *Catalysis Today*, 2017, **280**, 220-231.
55. O. Custance, S. Brochard, I. Brihuega, E. Artacho, J. M. Soler, A. M. Baró and J. M. Gómez-Rodríguez, *Phys. Rev. B*, 2003, **67**, 235410.
56. A. J. Martinez-Galera and J. M. Gomez-Rodriguez, *J. Phys. Chem. C*, 2011, **115**, 11089-11094.
57. I. Horcas, R. Fernandez, J. M. Gomez-Rodriguez, J. Colchero, J. Gomez-Herrero and A. M. Baro, *Rev. Sci. Instrum.*, 2007, **78**, 013705.
58. A. Gimeno, P. Ares, I. Horcas, A. Gil, J. M. Gomez-Rodriguez, J. Colchero and J. Gomez-Herrero, *Bioinformatics*, 2015, **31**, 2918-2920.
59. A. J. Martinez-Galera, U. A. Schroder, C. Herbig, M. A. Arman, J. Knudsen and T. Michely, *Nanoscale*, 2017, **9**, 13618-13629.
60. H. P. Koch, R. Laskowski, P. Blaha and K. Schwarz, *Phys. Rev. B*, 2012, **86**, 155404.
61. A. Goriachko, Y. He, M. Knapp, H. Over, M. Corso, T. Brugger, S. Berner, J. Osterwalder and T. Greber, *Langmuir*, 2007, **23**, 2928-2931.
62. P. Avila, M. Montes and E. E. Miro, *Chem. Eng. J.*, 2005, **109**, 11-36.
63. C. S. Song, *Catal. Today*, 2002, **77**, 17-49.
64. A. Russell and W. S. Epling, *Catal. Rev.-Sci. Eng.*, 2011, **53**, 337-423.
65. C. K. Narula, L. F. Allard, G. M. Stocks and M. Moses-DeBusk, *Sci Rep.* 2014, **4**, 7238.